Sedimentary Geology 210 (2008) 1–10

Contents lists available at ScienceDirect

Sedimentary Geology

journal homepage: www.elsevier.com/locate/sedgeo

Estimation of grain-size distributions and associated parameters from digital images of sediment

Daniel Buscombe

School of Geography, University of Plymouth, Plymouth, PL4 8AA, UK

ARTICLE INFO

Article history:
Received 30 June 2007
Received in revised form 11 March 2008
Accepted 18 June 2008

Keywords:
Grain size
Grain size distribution
Digital image
Beach
Percentiles

ABSTRACT

A new technique to estimate the grain-size distribution (GSD) from a digital image of sediment is proposed, advancing the applicability of a suite of sedimentary 'look-up-catalogue' approaches originated by Rubin [Rubin, D.M., 2004. A simple autocorrelation algorithm for determining grain size from digital images of sediment. Journal of Sedimentary Research, 74(1): 160–165]. The outputs of an automated procedure to estimate the GSD from digital images of sediment are examined with reference to the distributions obtained from both manually sieving the corresponding sediment samples, and axial measurements made on the grains in the images. Measures of grain-size obtained from the imaging procedure correlate very well with grain-size measures derived from both the number-frequency and mass-frequency curve. As expected the GSD obtained from the new automated approach, based on kernel density, compared better with point counts because of a shared two-rather than three-dimensionality. The GSD shape is not always mimicked exactly, however the percentiles obtained from the cumulative GSD compare well with those from sieved distributions, which allow for the first time computation of graphical sorting and skewness from digital images of sediment which are accurate reflections of those measures obtained for point-count and sieved samples. The new approach allows for realistic GSDs from which the residual can be computed, thus a numerical criterion upon which the grain-size distribution from an image can be accepted or rejected. Finally, a method is presented whereby two-dimensional autocorrelogram fields are derived from image power spectra. Ellipsoids are fitted to isolines of autocorrelation coefficients, and from this the dominant axial lengths and orientation of these isolines which could facilitate computation of major and minor axis lengths of grains in sample images, as well as their dominant orientation. In turn, this could allow for parameterisation of axial ratios for parameterisation of 2D shape. Such analysis is completely automated, rapid and non-intrusive.

1. Introduction

Particle-size analysis involves obtaining a grain-size distribution from a sample of sediment. There are several problems associated with particle-size analysis using traditional methods such as sieving, settling, and laser-diffraction. The first is that these techniques are not equivalent, because they measure slightly different things, and thus the computed grain-size distributions and sample statistics differ. The measurement techniques are themselves stochastic (Winkelmolen, 1982), and cannot straddle the size fractions from mud to cobbles. Settling and laser-diffraction, for example, are useful for muds, silts and sands, but not gravels or cobbles. A second problem with particle-size analysis through traditional methods is that they produce mass-frequency rather than number-frequency curves. The number of individual particles remains unknown, thus precluding the use of ordinary statistical measures of fit such as chi-squared, between measured grain-size distributions and parametric models. A related problem is that traditional measurement practices require the grain-size information is grouped, rather than continuous, which makes the numerical solution to some probability density functions difficult or impossible.

A potentially major disadvantage of particle-size analysis for sedimentary characterisation of beds under flows is that samples must be manually removed from the depositional environment, and often brought back to the laboratory for detailed analyses. Not only is this laborious, making obtaining a grain-size distribution a lengthy process, by removing the sample from the environment any information on the spatial configuration of those grains on the bed is lost. Thus a methodology which can estimate grain-size distributions remotely is required.

Obtaining grain-size measures from digital images of sediment beds has, for the reasons outlined above, long been an attractive option (e.g. Ibekken and Schleyer, 1986; Butler et al., 2001). Theoretically, obtaining a grain-size distribution from an image should be less laborious and time-consuming than traditional methods, if the process can be automated. The bed remains intact, and if the same image analysis procedure could be applied to a whole range of sedimentary

E-mail address: daniel.buscombe@plymouth.ac.uk.

0037-0738/$ – see front matter © 2008 Elsevier B.V. All rights reserved.
doi:10.1016/j.sedgeo.2008.06.007

beds, from muds to cobbles, then the size distributions obtained would be directly equivalent.

Unfortunately, early attempts at obtaining grain-size information from photographic images were not automated, and thus were not an attractive alternative to traditional means. They were limited in scope to gravels and cobbles. The modern generation of image analysis methods, using digital images, are designed to be automated and thus fast and efficient. These algorithms (e.g. Butler et al., 2001; Sime and Ferguson, 2003; Graham et al., 2005) use sophisticated image segmentation and thresholding and give a robust estimate of grain-size distributions for coarse gravels by segmenting each individual grain, and return the axial and areal properties of each. However, problems remain with these methods, such as for use on sediment beds composed of grains difficult to segment. For example, a range of colours/mineralogies, or small gravel or sand, or where pebbles have inter-granular aberrations such as pock-marks, abrasion hollows and scratches.

Due to the problems associated with the automated particle-size analysis of images of sand beds, Rubin (2004) proposed a new method for estimation of grain-size based on the spatial distribution of image intensity. In images of relatively large sediment, neighbouring pixels have similar intensity values for a greater distance than images of smaller grains. Thus the spatial autocorrelation of an image is sensitive to the relative size of objects in that image (Lin, 1982). Rubin (2004) suggested that, given careful calibration consisting of compiling correlograms for images containing known sediment sizes, reliable estimates of mean grain-size could be found by comparing the correlogram from a sample image with the calibration catalogue, through a simple least-squares problem. The technique has been validated for use on sand-sized sediment by Rubin et al. (2006, 2007) and Barnard et al. (2007). The latter study showed that mean grain-size could be estimated to within 10% of the mean grain-size as determined by point counts. Buscombe and Masselink (in press) achieved similar accuracy for fine-medium gravels.

There is a growing body of work which has begun to utilise these methods in experimental studies in fluvial and littoral settings (Gallagher et al., 2006; Rubin et al., 2006; Ruggiero et al., 2007; Barnard et al., 2007; Mustain et al., 2007). However, in order for the outputs and range of applicability of these statistical automated techniques to be on a par with the outputs from more traditional grain-size analysis techniques, they must accurately reproduce the entire grain-size distribution (GSD), or at least percentiles of that distribution, in addition to accurately quantifying mean/median sediment size. Only in doing so will physically meaningful and testable parameters (such as sorting, skewness, etc) be derived, which will drive progress in developing/testing theory or models that relate spatial and temporal gradients in sedimentation and grain-size distributions. The purpose of this communication is to propose and validate an algorithm designed to determine not only the mean grain-size (Rubin, 2004; Rubin et al., 2007; Buscombe and Masselink, in press), but also the entire GSD from a digital image of sediment.

2. Methods

2.1. LUC methods

Following Rubin (2004) and Rubin et al. (2007), a sample image (e.g. Fig. 1) is subjected to a numerical technique which is sensitive to the statistical distribution of grain-sizes within that image. This generates an array of numbers, which is the signature of the size information obtained within the sediment image. The procedure then involves 'looking-up' the elements of the sample in a calibration catalogue of such numerical signatures associated with different sized sediment, and, based upon their location, returning output values interpolated within the elements of the catalogue. The catalogue becomes a 'look-up table', a data structure used to find solutions based on several pre-computed solutions. The reader is referred to Rubin (2004) and Buscombe and Masselink (in press) for a more detailed discussion on the principles involved, as well as methodological guidelines for the collection and analysis of calibration and sample images. There are a number of numerical routines which may be employed for the purposes at hand (Buscombe and Masselink, in press), however the most common is the autocorrelation approach of Rubin (2004).

Fig. 1. An example image taken of gravel sized sediment following the recommendations of Buscombe and Masselink (in review).

The autocorrelation function (r), used as a measure of two-dimensional spatial independence, could be sensitive to the size of grains within images of sand, and thus, given careful calibration, could be used to derive a rapid, yet accurate, measure of sediment size. Positive spatial autocorrelation is the tendency for objects closer together to be more similar than objects further apart. For images of natural beds, pixels patches covering larger grains are more similar for a longer distance than pixel patches covering smaller grains. The general linear equations for the problem of solving for the proportions of calibrated sizes that collectively give the best fit to a given sample's numerical signature are given by (modified from Rubin (2004)):

$$\begin{aligned} a_{(1,1)}x_1 + a_{(1,2)}x_2 + \ldots a_{(1,m)}x_m &= b_1 \\ a_{(2,1)}x_1 + a_{(2,2)}x_2 + \ldots a_{(2,m)}x_m &= b_2 \\ &\vdots \\ a_{(n,1)}x_1 + a_{(n,2)}x_2 + \ldots a_{(n,m)}x_m &= b_n \end{aligned}$$

where $x_1 \ldots x_m$ are the proportion of size fraction 1:m in the sample, $a_{n,1} \ldots a_{n,m}$ are the numerical signature values for lags 1:n of the calibration samples 1:m, and $b_1 \ldots b_n$ are the observed numerical values for lags 1:n in the current sample. This linear problem is therefore defined simply, where a is the sample array (a column vector with n components) and C is the $m \times n$ calibration catalogue, by:

$$a(n) = \sum_{k=1}^{m} C(n,k) \times X(n) \tag{1}$$

where the vector solution $X = x_1 : x_n$ is the one that minimises the sum of squared errors between C and a, or $(a - CX)^T \times (a - CX)$, where T denotes matrix transpose. A matrix division of a into C finds the solution x for every catalogue sediment size, s, by Gaussian elimination. This minimises the residual between C and a, or $\min[||CX - a||]$ where $||\ldots||$ denotes the matrix norm or largest singular value. However, such a solution is not desirable because it may be positive or negative, which is not physically realistic. Alternatively, the least-squares result is commonly found by interpolation of a within C indexed at s, producing m values, i.e. solving for every lag, m, rather than every size, s. The mean of the resulting vector has been shown to be a good estimate of mean grain-size (Rubin et al., 2007; Barnard et al., 2007; Buscombe and Masselink, in press).

2.2. A grain-size distribution

Whilst the interpolation method is reliable for ensemble statistics such as mean size, solving for every lag rather than every size means that GSDs are not explicitly obtained. The best numerical solution is the one which minimises the residuals, or min(||$CX-a$||). Rubin (2004) used an (iterative) optimisation routine (Lawson and Hanson, 1974) to find the grain-size T 'distribution', a vector solution which minimises $(a-CX)^T\times(a-CX)$ such that $x\geq 0$. The advantage is that physically unrealistic values are avoided, but it is computationally more intensive, more unstable, and distributions thus obtained are dissimilar to natural size-distributions. It is possible that by further constraining the problem, such as an upper bound, better estimates of distributions may be found. However, with further constraints the optimisation problem becomes even more computationally intensive, and distributions thus obtained are likely still to be dissimilar to natural size-distributions.

For example, distributions were obtained from the imaged sample in Fig. 1 using the autocorrelation algorithm detailed in Rubin (2004), modified by Buscombe and Masselink (in press), and calculated using both 'least-squares' and 'least-squares with non-negativity' methods. The outputs may be seen in Fig. 2 (dashed and dotted line, respectively), compared to the measured distribution for that sample as determined by dry mechanical sieving (solid line) at $1/4\Phi$. To ensure a fair comparison, the sieves used were identical to the fractions represented by the calibration catalogue used for the computations. This sample is typical of the behaviour exhibited by the two respective distribution-estimation methods on digital images of sediment: the least squares method tends to produce a unimodal, unrealistically well sorted distribution; and the least-squares with non-negativity method produce statistical artifacts such as a 'blocky', multimodal distribution. Often the reality lies somewhere between the two, as in Fig. 2. While estimates of median size (D_{50}) closely match the real sample, derived measures such as sorting and skewness are often wildly inaccurate using these distribution estimation methods.

An alternative approach is to arrive at the vector solution x using a least squares approach, then to use x to compute a smooth probability density function (pdf) using a non-parametric kernel density estimation routine (otherwise known as a Parzen method), which takes the form:

$$f(x)=\frac{1}{nh}\sum_{i=1}^{n}K\left(\frac{x-x_i}{h}\right) \tag{2}$$

with kernel K, bandwidth h, and number of points n. The centre of the kernel is placed over every data point, and the influence of the datum is spread about its neighbourhood, depending on the shape of the kernel. The contribution of each datum is then summed to an overall estimate, thus removing the dependence on the end points of the bins. The kernel can take on several forms (similar to wavelets or digital filters). The bandwidth (or 'scaling factor') controls how far the probability mass is spread around a datum, thereby controlling the smoothness of the probability density estimate. In other words, replace each observation x_i by a copy of the function K, shifted so that it is centred at x_i, and scaled by a factor h. Kernel estimation is conducted using non-negativity constraints by providing a bounded support where only positive values can be recorded.

A lot of research has focussed on the optimal value for the bandwidth parameter (Sheather and Jones, 1991) since the quality of a kernel estimate generally depends less on the shape of the K than on the value of its bandwidth. In numerical trials it was found that the 'generalized cross entropy (GCE)' method of Botev (2006) to be most reliable, closely followed by the (computationally much simpler) 'rule-of-thumb' formula suggested by Bowman and Azzalini (1997):

$$h=\left(\frac{4}{3n}\right)^{1/5}\sigma \tag{3}$$

where σ is the standard deviation of the histogram of X. Trials using different kernels on sample images in this study deemed a 'normal' or 'Gaussian' kernel to be suitable, given by (Bowman and Azzalini, 1997), given by:

$$K(x)=\frac{1}{\sigma\sqrt{2\pi}}e^{-x^2/2\sigma^2} \tag{4}$$

The kernel may be estimated directly from x, it may assume a given probability density function (e.g. normal or log-normal), and supports

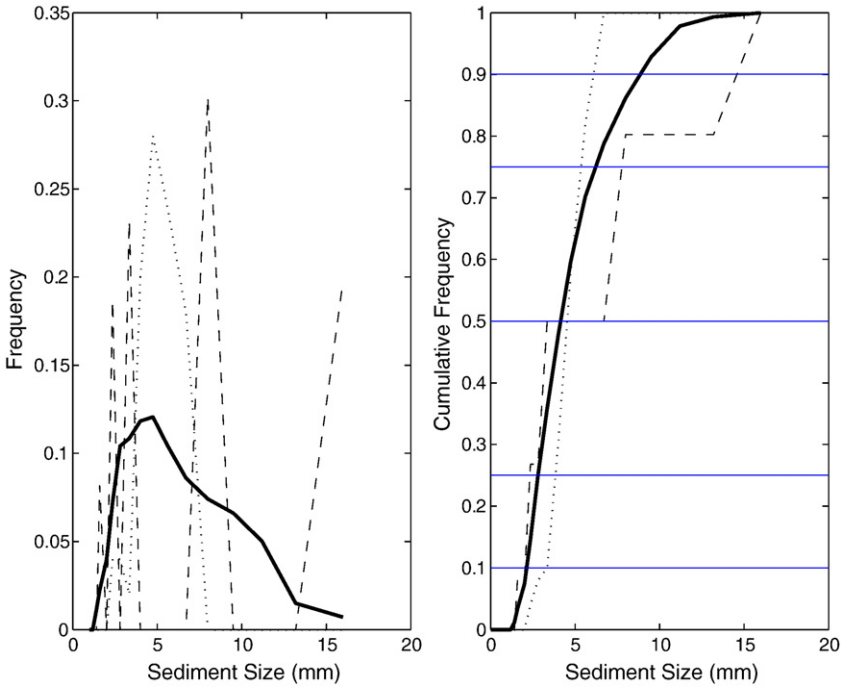

Fig. 2. A Comparison of GSDs and cumulative GSDs obtained from sieving (solid line), and imaging the same sample (Fig. 1). Frequencies are normalised to sum to unity. Dotted lines indicate the GSD derived using a linear least squares and histogram approach; and dashed lines indicate the distribution obtained from a linear least squares with non-negativity constraints approach. Solid horizontal lines indicate commonly used percentiles (10, 25, 50, 75 and 90).

may be specified such as only allowing for positive grain-sizes. Importantly, the technique converts a solution array x indexed at m, to a solution of proportions indexed at s which sums to unity whilst conserving probability mass, i.e. a grain-size distribution. It therefore makes interpolated solution x amenable to measures of the extent to which the solution minimises the residual between a and C, which is a measure of the numerical 'fit' in the solution of the least-squares problem. As such, it can be a criterion upon which the grain-size distribution from an image can be accepted or rejected.

The distribution estimated by the kernel density method may be seen in Fig. 3 (dashed line) with reference to the sieved sample (solid line). The shapes closely agree, as do the percentiles in the cumulative distribution. Accordingly, the derived parameters from the distribution estimated by the kernel method are in better agreement with those derived from the sieved distribution. On this occasion, the kernel method performs better for size, sorting and kurtosis (but not for skewness, because it underestimates the coarse tail). Note that this sample was chosen at random: some fits are considerably better than this, and others marginally worse.

3. Validation

Fifty sediment samples were collected from a gravel beach, and subsequently dried; imaged (according to the method outlined in Buscombe and Masselink (in press)), modified from the method proposed by Rubin et al. (2006)); and sieved at 1/4Φ between 32 mm and 1.4 mm. Calibration catalogues were compiled for the autocorrelation technique with images of sieved sediment in the corresponding sizes. Graphical size, sorting, skewness and kurtosis were computed from the sieved distributions (Folk and Ward, 1957). Images were analysed using the kernel approach outlined above to obtain a grain-size distribution, using bandwidths given by [3]. An image will be processed in ≤1 min on a ≥1 GHz processor, so batch processing images is very quick.

Barnard et al. (2007) compared their automated results with grain-size based on visual point counts of grains in the same image, and using this approach, demonstrated that much of the discrepancy between mean grain-size measured from sieving of samples and calculated from surface images is due to differences between size of surface and sub-surface grains rather than due to errors in the grain-size algorithm, because surface grains are only a subset of a larger population that is obtained in a sample manually obtained. This approach has also been adopted here. The major axes of grains in each image were measured manually using Matlab ® software (see Fig. 4 for chords manually drawn across the major axes of grains). The field of view (FOV) of the image, in mm/m, may be found using (Gonzalez and Woods, 2002):

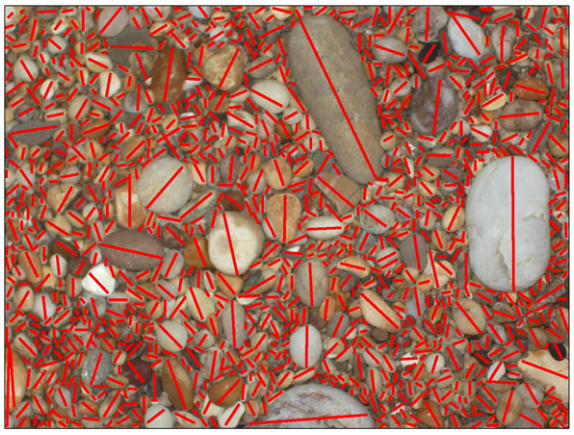

Fig. 4. Major and minor axes were estimated visually from images of sediment to build a histogram of sizes. An example of major axis chords on an image of grains is shown here.

$$\mathrm{FOV} = 17.15\left(\left[2\arctan\left(\frac{c}{2f}\right)\right] \times \left[\frac{180}{\pi}\right]\right) \quad (5)$$

where c and f are the CCD (imaging device) size and focal length, respectively, in millimetres. Scaling by the pixel dimensions of the image in the vertical and horizontal directions allows for the calculation of resolution in pixels per millimetre, thus calculation of the lengths of features within the image are possible.

Each derived parameter from image and sieving methods were analysed for statistical similarity. Tables 1 and 2 list correlation coefficients (r) for each parameter set, as well as F-ratio and a T-test

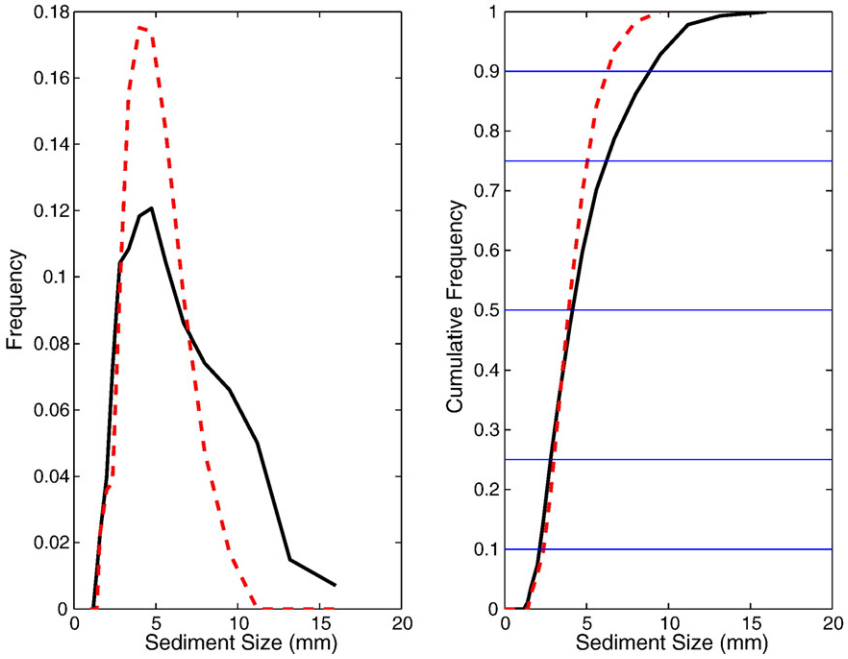

Fig. 3. A Comparison of GSDs and cumulative GSDs obtained from sieving (solid line), and imaging the same sample (Fig. 1). Frequencies are normalised to sum to unity. Dashed lines indicate the distribution obtained using a kernel density estimation approach on the linear least squares solution vector. Solid horizontal lines indicate commonly used percentiles (10, 25, 50, 75 and 90).

Table 1
Image kernel density approach versus distribution from point counts

Parameter	Correlation	Mean absolute deviation	*F*-ratio	*T* test
D_{90}	0.81	2.99	89.05	9.56
D_{10}	0.8	0.21	86.89	9.23
D_{50}	0.92	0.82	249	16.26
F & W graphical mean	0.93	0.67	288.48	17.52
F & W graphical skewness	0.83	0.57	112.45	10.3
F & W graphical kurtosis	0.61	0.77	28.26	5.33
F & W graphical sorting	0.74	0.27	57.72	7.62

All parameters are significant at 95%.

Table 2
Image kernel density approach versus distribution from sieving

Parameter	Correlation	Mean absolute deviation	*F*-ratio	*T* test
D_{90}	0.69	1.54	43.52	6.6
D_{10}	0.82	0.24	95.64	9.92
D_{50}	0.89	0.61	185.26	13.52
F & W graphical mean	0.9	0.35	210.3	14.3
F & W graphical skewness	0.57	0.43	23.53	4.81
F & W graphical kurtosis	0.53	0.88	19.11	4.33
F & W graphical sorting	0.64	0.34	34.65	5.77

All parameters are significant at 95%.

value to determine the statistical significance of the correlation coefficients under:

$H_0 : r = 0$

$H_1 : r \neq 0$.

That is, whether the observed sample correlation is significantly different from zero. A *t* test for significance of *r* is given by:

$$t = \frac{r\sqrt{n-2}}{\sqrt{1-r^2}} \quad (6)$$

which has *n*-2 degrees of freedom, and which was tested at the α=0.05 (5%) level. With v_1=48, this means a critical value for *t* of 2.011. The results may be seen in Table 1 for the image kernel method versus distributions obtained from point counts, and in Table 2 for the image kernel method versus distributions obtained from sieving. All computed statistics were significant at 95%, although greater correlation was found between the distributions obtained from the image kernel method compared with point counts (Table 1) as opposed to the sieve method (Table 2). Results for mean and median size are shown in Fig. 5. The kernel image method compares well with both sieve and point count approaches, according to correlation coefficients and mean absolute deviations. Results for D_{90} and D_{10} are shown in Fig. 6. There is a tendency to under-estimate these percentiles compared to measures computed from sieved distributions, suggesting that whilst there is no systematic bias in the calculation of the mean/median, there is for percentiles on the distribution tails. Interestingly, however, the bias is similar for both point count and sieved methods. Results for graphical (percentile-derived) sorting and skewness are shown in Figs. 7 and 8, respectively. These results are particularly encouraging. As expected from Barnard et al. (2007), the statistics computed from the kernel method consistently compare better with those from point counts on the same images.

Following Sime and Ferguson (2003) and Graham et al. (2005), the performance of kernel algorithm for seven percentiles estimated from the image distributions using mean error, mean-square error and irreducible random error. These are defined below in Table 3 where p_s and p_i denote the percentile value for the counted/sieved and imaged distribution (in Ψ units), respectively, and *n* is the sample size given as number of images (50) multiplied by the number of percentiles (7) tested. The irreducible error (Table 3) is greater than the values quoted by Graham et al. (2005) (0.0691–0.089 Ψ, or ≈1.05 mm), but comparable than those quoted by Sime and Ferguson (2003) (0.253–0.26 Ψ, or ≈1.19 mm), in their studies utilising image object detection algorithms on much larger gravels. The quoted values here are based on a greater number of tested percentiles. The irreducible random error is smaller for the kernel density approach

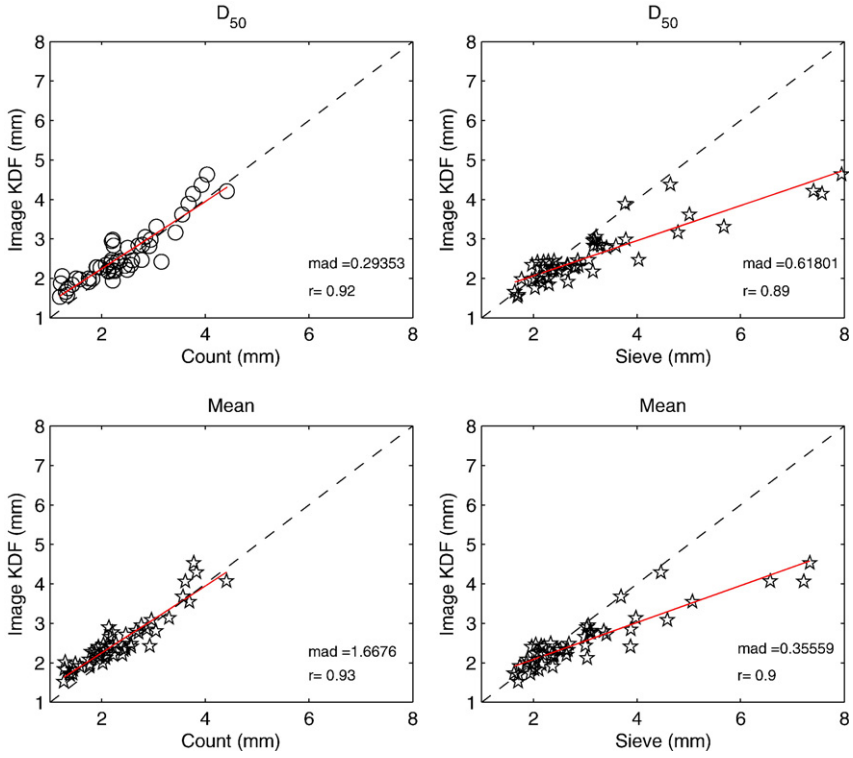

Fig. 5. Top row: D_{50} from image kernel GSDs compared with point count GSDs (left) and sieve GSDs (right). Bottom row: mean size from image kernel GSDs compared with point count GSDs (left) and sieve GSDs (right). KDF stands for 'kernel density function'.

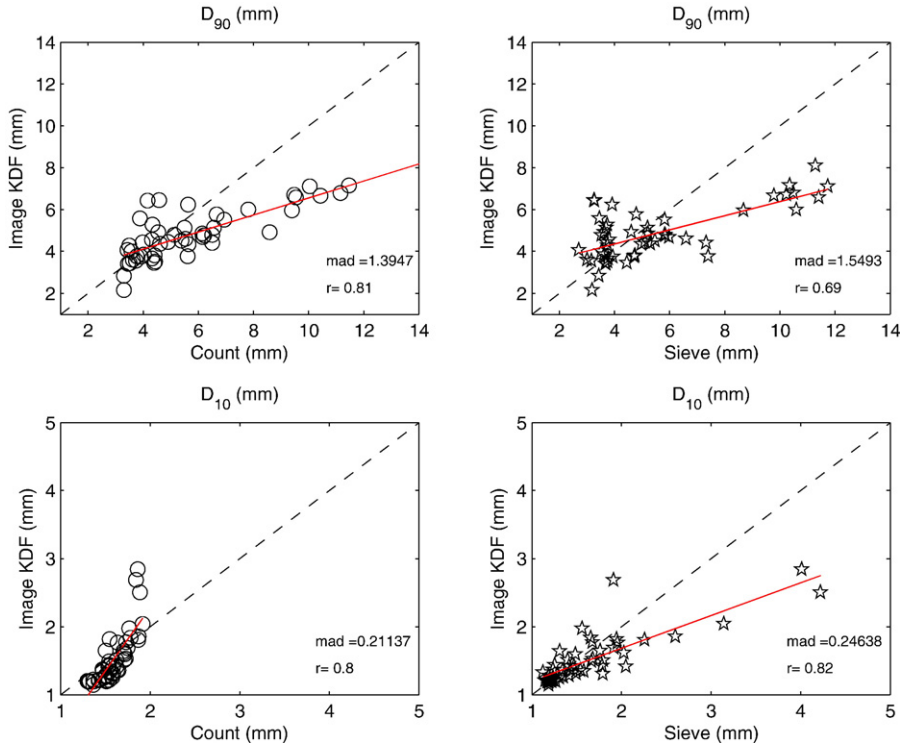

Fig. 6. Top row: D_{90} from image kernel GSDs compared with point count GSDs (left) and sieve GSDs (right). Bottom row: D_{10} from image kernel GSDs compared with point count GSDs (left) and sieve GSDs (right). KDF stands for 'kernel density function'.

compared to point counts (0.169 Ψ or ≈1.12 mm), as compared to sieving (0.255 Ψ or ≈1.19 mm).

4. Major and minor axis lengths and orientation

The autocorrelation function employed in the spatial domain is sensitive to the starting point and direction through which the function is applied. Due to the presence of a mixture of grain-sizes and shapes within the calibration images, differentiation of closely-sized fractions of material can be difficult, which often means that the calibration catalogue must be truncated at a relatively short lag, beyond which there is non-differentiation. Short correlograms threaten the statistical reliability of the computed mean grain-size and grain-size distribution. Buscombe and Masselink (in press)

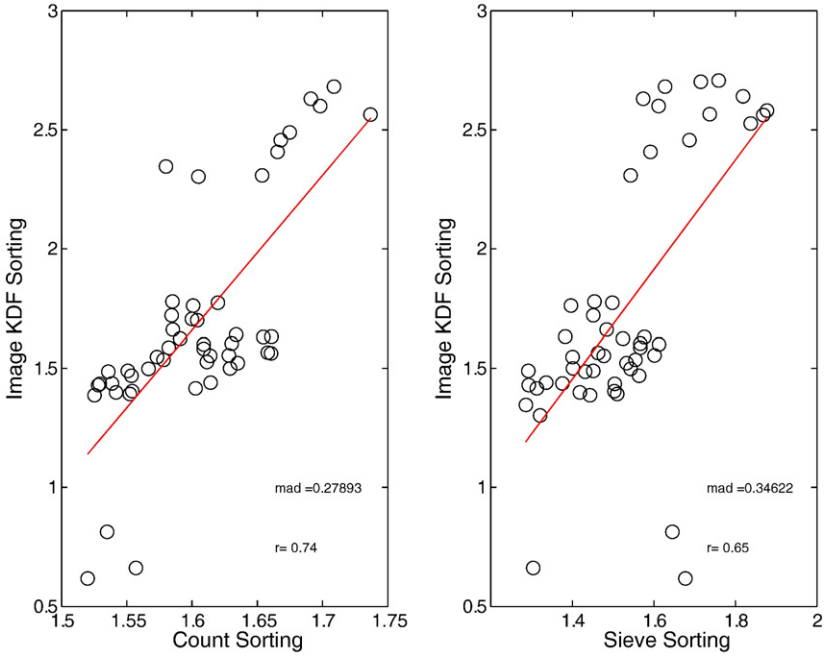

Fig. 7. Graphical sorting from image kernel GSDs compared with point count GSDs (left) and sieve GSDs (right). KDF stands for 'kernel density function'.

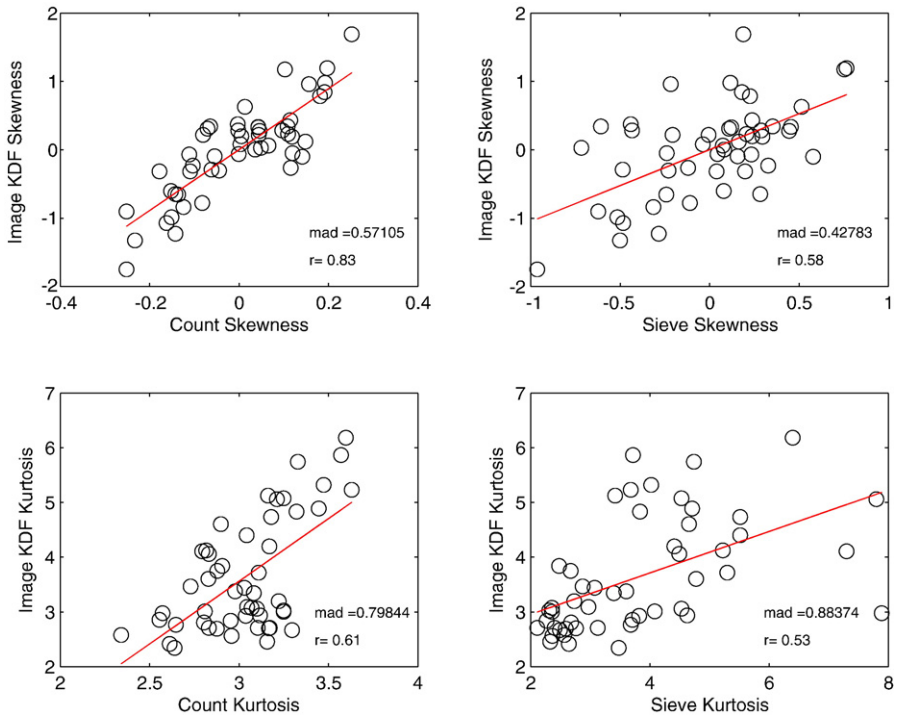

Fig. 8. Top row: graphical skewness from image kernel GSDs compared with point count GSDs (left) and sieve GSDs (right). Bottom row: graphical kurtosis from image kernel GSDs compared with point count GSDs (left) and sieve GSDs (right). KDF stands for 'kernel density function'.

explored the use of spectral indices of spatial (in)dependence, concluding that whereas the spatial domain approach is sensitive to the direction and starting point from which it is applied (due to the presence of various sizes and shapes within the calibration images), the spectral domain maps image intensity at all scales and directions within the image thus it is less sensitive to mixtures of shapes and sizes in calibration images which should ideally be homogenous, although in practice this is impossible to achieve. It may be possible, therefore, to create calibrations which distinctly differentiate over longer lags. In turn, this may allow for more calibration size-fractions, a better conditioned linear least-squares problem, greater statistical reliability (a larger sample size, both in terms of grain size fractions and computed lags), and better estimates of grain-size and moments of the distribution.

Preston and Davis (1976) and Lin (1982) discuss the utility of two-dimensional Fourier transforms and autocorrelograms, respectively, on characterising texture from binarised electron microscope images of sandstone thin sections. The zero-shifted 2D power spectrum maps intensity as a function of all frequencies and directions within the image. If intensity is measured along an arbitrary radius from the centre of the power spectrum (e.g. Fig. 9) to the edge, that is equivalent to a one-dimensional power spectrum of the image in that direction. As noted by Buscombe and Masselink (in press), this observation is essentially the same as found by Rubin (2004) with an autocorrelation function: shallow sloped autocorrelograms indicate relatively coarse sediment because the images are self-similar over greater distances.

A two-dimensional autocorrelogram may be obtained from the two-dimensional power spectrum. The Wiener–Khinchin theorem states that the power spectral density, S, of a stationary random process, in this case the spatial distribution of intensity within the image, is the Fourier transform of the autocorrelation function (Petrou and Bosdogianni, 1999). The power spectrum and the

Table 3
Errors associated with seven percentiles (10, 16, 25, 50, 75, 84 and 90), following Graham et al. (2005)

Parameter	Image kernel vs point count	Image kernel vs sieve
$\bar{b}=1/n\Sigma(p_s-p_i)$	0.663Ψ	0.20Ψ
$E_{ms}=1/n\Sigma(p_s-p_i)^2$	0.609Ψ	0.2958Ψ
$e^2=E_{ms}-b^2$	0.169Ψ	0.255Ψ

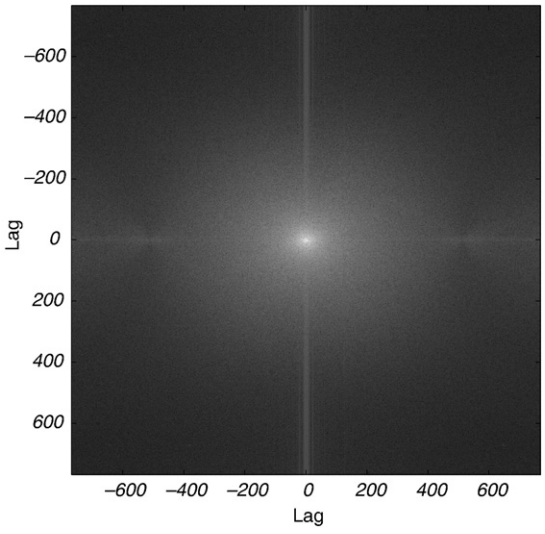

Fig. 9. A digital image of sediment in the frequency domain. Low frequencies towards the centre of the image (origin) correspond to the slowly-varying components of the image and are associated with most power. Further from the origin are the high frequencies associated with faster changes in the image. Grains which are strongly oriented in a certain direction show are elongated fields of light in their power spectra.

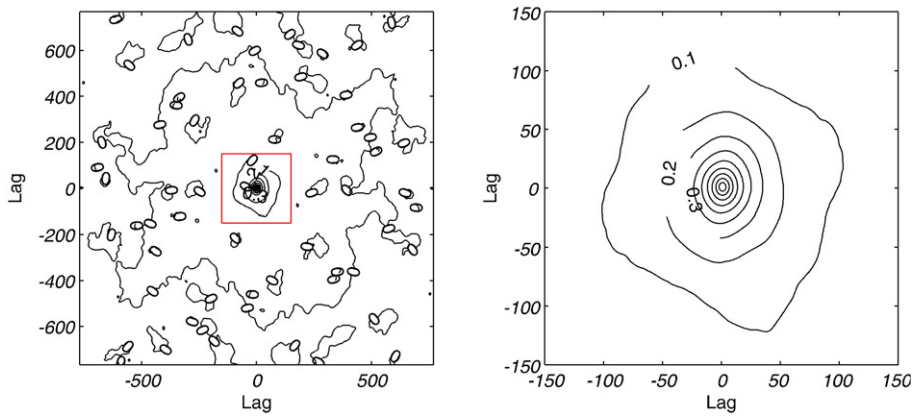

Fig. 10. Left: The autocorrelogram computed from the power spectrum Fig. 9 and contoured. Note that autocorrelation decays to zero radially and rapidly from the origin. The area inside the box is seen in detail on the right panel.

autocorrelation function r_x are given by, where x_n denotes the whole integers of a digital image.

$$S_x(f) = \sum_{k=-\infty}^{\infty} r_x(k)e^{i2\pi kf} \tag{7}$$

$$r_x(k) = E[x(n)x^*(n-k)] \tag{8}$$

where k is the lag index, i is the imaginary unit, e is the base of the natural logarithm, f is the frequency index, E denotes mathematical expectation, and * denotes complex conjugate. The two-dimensional autocorrelogram of a de-meaned image is thus the inverse Fourier transform of its two-dimensional power spectrum, normalise by its value at zero lag, which is the total power in the spectrum (Petrou and Bosdogianni, 1999).

The two-dimensional power spectrum and autocorrelogram of a digital image of sediment through every direction within the image appears as a field of light radiating outward from the centre (Fig. 9). In other words, power spectral density decreases exponentially as a function of wavelength, as autocorrelation decreases exponentially as a function of lag. The corresponding two-dimensional autocorrelogram of the power spectrum mapped in Fig. 9 is contoured in Fig. 10. In a square image, elongation of this field of light in any direction indicates anisotropy in the spatial frequency distributions of image intensity. A perfectly circular closed contour would, on the other hand, indicate perfect isotropy in the features within the image, as would be achieved by uniformly-circular grains. The closed contours are elliptical rather than circular which indicates there is some anistropy in the grains, or in other words, axial dimensions of grains are unlikely to be equal.

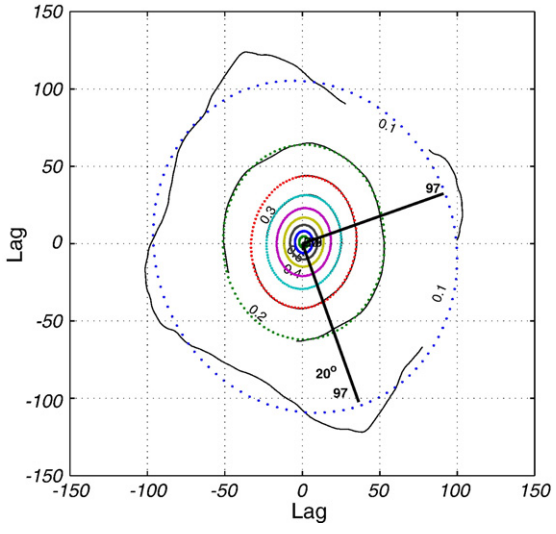

Fig. 11. The autocorrelogram of Fig. 10 contoured and ellipses fitted (dashed lines) using Fitzgibbon et al. (1999). The length (in lags) and orientation (in degrees, relative to the top of the image) of the correlogram surface shown for the outer contour (r=0.1) have been computed using the method described in the text.

A two-dimensional autocorrelogram allows the construction of an LUC in the frequency domain. Potentially, this could be done for all orientations in the original image, although the amount of redundant information would render such an exercise intractable in any practical sense. However, it could be useful in revealing information on anisotropy in image intensity from the two or three dominant orientations of features within the image, which could yield information on the major and minor axes of grains within the image. A method for constructing such calibration catalogues is outlined below.

An ellipse may be fitted to each specified contour of autocorrelation, r, in order to obtain its minor and major axial length (in lags), and orientation. For example, Fig. 11 shows ellipses fitted to contours of r=0.1–0.9. The major and minor axial lengths, in lags, for r=0.1 are shown, as well as the principal axis orientation relative to N–S in the image. Cataloguing these r as a function of both lag and s should enable the construction of two calibration catalogues: one for 'major', and one for 'minor' axial lengths.

An ellipse is fitted to a contour described by the coordinates $[x,y]$ using a second-order polynomial given by:

$$F(x,y) = ax^2 + bxy + cy^2 + dx + ey + f = 0 \tag{9}$$

where $\mathbf{a}=[a,b,c,d,e,f]^T$ are coefficients. Following Fitzgibbon et al. (1999), the coefficients are found by solving the following minimisation problem:

$$\min||Da||^2 \tag{10}$$

subject to $\mathbf{a}^T C\mathbf{a}$, where design matrix D is defined as:

$$D = \begin{vmatrix} x_1^2 & x_1y_1 & y_1^2 & x_1 & y_1 & 1 \\ \vdots & \vdots & \vdots & \vdots & \vdots & \vdots \\ x_n^2 & x_ny_n & y_n^2 & x_n & y_n & 1 \end{vmatrix}$$

and constraint matrix C is given as:

$$C = \begin{vmatrix} 0 & 0 & 2 & 0 & 0 & 0 \\ 0 & -1 & 0 & 0 & 0 & 0 \\ 2 & 0 & 0 & 0 & 0 & 0 \\ 0 & 0 & 0 & 0 & 0 & 0 \\ 0 & 0 & 0 & 0 & 0 & 0 \\ 0 & 0 & 0 & 0 & 0 & 0 \end{vmatrix}.$$

The solution to Eq. (10) is then given by:

$$Sa = \lambda Ca \tag{11}$$

where λ are the minimal non-negative eigenvalues, and where scatter matrix, S, is D pre-multiplied by its transpose, or $S=D^TD$. Ellipse angle θ, relative to the N-S axis in the image, is given by:

$$\theta = \arctan^*(b/2, (a-c)/2) \tag{12}$$

where $\arctan^*$ is the four-quadrant arctangent. The major and minor 'axes' are then found by:

$$r_1 = 1/\sqrt{(\varsigma^*_1)} \tag{13}$$

$$r_2 = 1/\sqrt{(\varsigma^*_2)} \tag{14}$$

where $\varsigma = 1/(\epsilon^T E \times \epsilon - f)$, using translations given by:

$$E = [a, b/2]^T [b/2, c]^T \tag{15}$$

$$\epsilon = -(2E)^{-1} [d, e]^T \tag{16}$$

(17)

and, where $s_1=\cos(\theta)$ and $s_2=\sin(\theta)$:

$$v_1 = (as_1^2) + (bs_1s_2) + (cs_2^2) \tag{18}$$

$$v_2 = (as_1^2) - (bs_1s_2) + (cs_2^2) \tag{19}$$

the origin of the ellipse is $[\epsilon(1),\epsilon(2)]$, and should be approximately zero. Fig. 11 shows an example of ellipses fitted to isolines of autocorrelation within a 2D spectral autocorrelogram.

5. Discussion

On the test images, the new GSD estimation technique was found to compare well with graphical measures obtained from both sieving and point counts. Similar to Barnard et al. (2007) who found that estimates of mean grain-size using autocorrelation were better correlated to those obtained from point counts, as opposed to sieving, here it was found that graphical moments from the new kernel density approach scaled better with point counts. The likely reason is that an image contains grains which are overlapping in a two-dimensional plane, and the sieving technique is three-dimensional. However, there is no quantifiable systematic bias introduced by the effect of proportions of grains 'hiding' in digital images of sedimentary beds, so one must conclude that it exerts equal effect on grains of all sizes.

The close agreements obtained here are a factor of at least four favourable elements. The first is that the quality of the images were checked beforehand, and images too dark or out of focus were discarded prior to analysis. The second is that the tested images were beach gravels, which are relatively well rounded. The third is that all samples tested were broadly unimodal. Finally, the calibration catalogue used for the autocorrelation method was large (19 grain sizes, and 50 lags — for comparison, Barnard et al. (2007) used a catalogue with 12 grain sizes and 20 lags), but still non-overlapping (each sediment size in the catalogue having distinct correlograms over 50 lags). Thus the sample size used for each kernel density estimation was large (50). The accuracy of the technique may be very sensitive to the number of lags over which the calibration curves representing different sediment sizes remain distinct. Results which are closer to those obtained by sieving should be achievable by averaging over several images (Rubin, 2004; Barnard et al., 2007) because the surface grains imaged in two-dimensions are only a subset of a larger population that is obtained in a (three-dimensional) grab sample which is subsequently sieved.

The kernel may be estimated directly from x, it may assume a given probability density function (e.g. normal or log-normal), and supports may be specified such as only allowing for positive grain-sizes. Importantly, the technique converts a solution array x indexed at some lags, to a solution of proportions indexed at some calibration sizes. It therefore makes interpolated solution x amenable to measures of the extent to which the solution minimises the residual between a and C, or 'goodness of fit'. However, the kernel-density technique for GSD estimation is sensitive to bandwidth estimation (Sheather and Jones, 1991). This study found that the methods of Bowman and Azzalini (1997) and Botev (2006) yielded satisfactory automated results, but the topic is widely discussed and there are others available (e.g. Silverman, 1986; Sheather and Jones, 1991; Scott, 1992) which might yield better results for certain problems.

Using the kernel distribution estimation technique outlined here, it is now possible to obtain reliable estimates of GSDs from digital images of sediment using the autocorrelation technique. Whilst the median/mean grain-size is the most commonly used parameter in sediment transport modelling, it is well known that the entire distribution and parameters of it are very useful for a large number of diverse purposes, including (to name but a few) environmental discrimination (e.g. Friedman, 1979) and reconstruction (e.g. Mohd-Lokman and Pethick, 2001; Knight et al., 2002); sediment provenance (e.g. McManus et al., 1980; Weltje and Prins, 2003); sediment trend modelling (e.g. McLaren and Bowles, 1985; Le Roux and Rojas, 2007); the bulk properties of grain aggregates such as sediment permeability (e.g. Krumbein and Monk, 1942); and sedimentological properties for activities of economic importance, for example beach fill design and monitoring (e.g. Stauble, 2007). Since the autocorrelation technique requires site-specific calibration and is most useful when a large number repeat measurements are required (Rubin et al., 2007), perhaps the most useful application of the kernel method for estimation of GSDs is where sedimentary parameters such as sorting and skewness may be used to infer, from field studies, contemporary fluvial, aeolian and coastal sediment transport processes.

Errors may be introduced to the autocorrelation method of Rubin (2004) due to the spatial nature of the algorithm and the heterogenous nature of grains with respect to size, shape and orientation. Spectral computations of autocorrelation may therefore be a better alternative in such cases where such non-uniformity lowers the signal:noise ratio and introduces errors into the 1D correlogram method (Buscombe and Masselink, in press). A method to estimate the lengths and orientations of major and minor 'axes' of grains in digital images of natural sediment beds has been proposed, using 2D spectral autocorrelograms. Whilst in need of further validation work, in addition to different calibration catalogues for calculation of minor and major axes length of grain within the image, it may inform the calculation of better grain-size distributions. A 2D spectral approach may even enable better differentiation of different grain-sizes within calibration images, and extend the length of those catalogues. Also note that frequency transforms are orders of magnitude faster than equivalent operations in the spatial domain. In turn, this approach could potentially allow for more calibration size-fractions, a better conditioned linear least-squares problem, greater statistical reliability (a larger sample size, both in terms of grain size fractions and computed lags), and better estimates of grain-size and moments of the distribution. Orientation of grains could be an important sedimentological parameter, especially if the collective body of 'digital grain size' or LUC techniques were extended to time-series from video cameras under flows.

6. Conclusions

In recent years advances have been made in the automated and accurate quantification of granular attributes from the statistical analysis of digital images of seabed and river sediments. Following Rubin (2004) a reasonable estimate of mean size can be obtained by solving a linear set of equations based on a sample image's autocorrelation profile, and those of several images of sediment of known grain-size. This approach is accurate in both sandy (e.g. Barnard et al., 2007) and gravelly (e.g.

Buscombe and Masselink, in press) environments. In this contribution, a new technique has been proposed for the estimation of a grain-size distribution (GSD) from a digital image of sediment. This method, based on non-parametric kernel density estimation, has been shown here to give realistic estimates of GSDs of coarse sand and fine gravel sediments, as compared to both point-counts and sieving. In turn, derived graphical percentiles from the cumulative distribution have allowed better approximations to sorting and skewness. Fifty sediment samples were tested, and were found to have statistically equivalent means, and coefficients of sorting, skewness and kurtosis based on graphical parameters, in comparisons both with sieved distributions and those obtained by point counts of grains on the images. The percentile errors are better or at least comparable to previous published studies using different image processing techniques on larger grain-sizes.

As expected, computed GSDs using the kernel approach outlined here compared better with GSDs obtained from point counts of grains on the images rather than those obtaining by sieving. Despite the theoretical difficulties in comparing GSDs obtained from two-dimensional images with GSDs obtained from sieving (see Sime and Ferguson (2003), Graham et al. (2005), Barnard et al. (2007) and Buscombe and Masselink (in press) for a discussion), these results are very encouraging. Estimates obtained using graphical methods for mean and sorting are good, and those obtained for skewness are adequate for most sedimentological purposes. Grain-size parameters based on moments are expected to be less accurate, especially skewness and kurtosis, because the exact GSD shape is not mimicked exactly.

In addition, a method has been proposed to extend the autocorrelation method of Rubin (2004) into two dimensions, using autocorrelogram fields. By contouring pre-defined values of autocorrelation, and using an ellipse-fitting function, it is shown that it is theoretically possible to determine the dominant orientations of grains within the image, and even to build calibration catalogues for major and minor axes of grains. Such work would require further validation, but could potentially open up 'digital grain-size' techniques into quantification of even more accurate grain-size distributions, and possibly measures of two-dimensional shape.

For the first time it has been demonstrated that an automated technique based on the statistical properties of digital images of sediment is able to provide a realistic grain-size distribution. A realistic GSD allows accurate estimates of GSD percentiles, which in turn allows the graphical parameters for sorting, skewness and kurtosis to be calculated. In this study the values obtained for sorting and skewness were good to reasonable, which broadens the applicability of rapid, remote and automated quantification of sand and gravel sediment for use in sediment trend and transport modelling, and detailed studies into spatial and temporal sedimentation in a number of sedimentary environments.

Acknowledgements

Thanks to Professor Gerhard Masselink for starting and sustaining my interest in this topic, and for reviewing an earlier draft of the paper. Thanks also to Isabelle Emmanuel and Tom Deacon who helped collect and sieve the samples, to Slapton Ley Field Studies Centre for their continuing support, and Tim Scott for his comments on an earlier draft. Thanks to Dr Dave Rubin and two anonymous referees for their helpful comments which considerably improved an earlier draft. This work was funded by a University of Plymouth SSB Faculty scholarship. Matlab® the computations detailed here are available from the author via email request.

References

Barnard, P.L., Rubin, D.M., Harney, J., Mustain, N., 2007. Field test comparison of an autocorrelation technique for determining grain size using a digital 'beachball' camera versus traditional methods. Sedimentary Geology 201 (1-2), 180–195.

Botev, Z., 2006. A novel non-parametric density estimator. Postgraduate Seminar Series, Mathematics (School of Physical Sciences). The University of Queensland.

Bowman, A., Azzalini, A., 1997. Applied smoothing techniques for data analysis. Oxford Statistical Science Series. Clarendon Press, Oxford.

Buscombe, D., Masselink, G., in press. Grain size information from the statistical properties of digital images of sediment. Sedimentology. doi:10.1111/j.1365-3091.2008.00977.x.

Butler, J.B., Lane, S.N., Chandler, J.H., 2001. Automated extraction of grain-size data from gravel surfaces using digital image processing. Journal of Hydraulic Research 39 (5), 519–529.

Fitzgibbon, A., Pilu, M., Fisher, R., 1999. Direct least square fitting of ellipses. IEEE Transactions on Pattern Analysis and Machine Intelligence 21 (5), 476–480.

Folk, R., Ward, W., 1957. Brazos River, Brazil: a study of the significance of grain size parameters. Journal of Sedimentary Petrology 27, 3–26.

Friedman, G.M., 1979. Differences in size distributions of populations of particles among sands of various origins-addendum to IAS presidential-address. Sedimentology 26 (6), 859–861.

Gallagher, E., MacMahan, J., Russell, P., Masselink, G., Auger, N., 2006. Morphological variability and grain size from digital images. Proceedings 30th International Conference on Coastal Engineering. ASCE, San Diego.

Gonzalez, R., Woods, R., 2002. Digital Image Processing, 2nd Edition. Prentice Hall, New Jersey.

Graham, D.J., Rice, S.P., Reid, I., 2005. A transferable method for the automated grain sizing of river gravels. Water Resources Research 41 (7).

Ibekken, H., Schleyer, R., 1986. Photo-sieving: a method for grain size analysis of coarse-grained, unconsolidated bedding surfaces. Earth Surface Processes and Landforms 11, 59–77.

Knight, J., Orford, J., Wilson, P., Braley, S., 2002. Assessment of temporal changes in coastal sand dune environments using the log-hyperbolic grain-size method. Sedimentology 49, 1229–1252.

Krumbein, W., Monk, G., 1942. Permeability as a function of the size parameters of unconsolidated sand. Transactions of the American Institute of Mineral and Metallic Engineers. In: Bear, J. (Ed.), Dynamics of Fluids in Porous Media. Elsevier, New York. 1972, 764 pp.

Lawson, C., Hanson, R., 1974. Solving Least Squares Problems. PrenticeHall.

Le Roux, J.P., Rojas, E., 2007. Sediment transport patterns determined from grain size parameters: overview and state of the art. Sedimentary Geology 202, 473–488.

Lin, C., 1982. Microgeometry I: autocorrelation and rock microstructure. Mathematical Geology 14, 343–360.

McLaren, P., Bowles, D., 1985. The effects of sediment transport on grain-size distributions. Journal of Sedimentary Petrology 55 (4), 457–470.

McManus, J., Buller, A.T., Green, C.D., 1980. Sediments of the Tay Estuary IV: bottom sediments of the lower and outer reaches of the Tay Estuary. Proceedings of the Royal Society of Edinburgh 78, 133154.

Mohd-Lokman, H., Pethick, J., 2001. Seasonality of sediment skewness as a geochronological tool for the Humber salt marshes, U.K. Wetlands Ecology and Management 9, 1–12.

Mustain, N., Griggs, G., Barnard, P., 2007. A rapid compatibility analysis of potential offshore sand sources for beaches of the Santa Barbara littoral cell. Coastal Sediments 07. Vol. 3. ASCE, New Orleans, pp. 2501–2514.

Petrou, M., Bosdogianni, P., 1999. Image Processing: The Fundamentals. Wiley, Chichester.

Preston, F., Davis, J., 1976. Sedimentary porous materials as a realization of a stochastic process. In: Merriam, D.F. (Ed.), Random Processes in Geology, pp. 63–86.

Rubin, D.M., 2004. A simple autocorrelation algorithm for determining grain size from digital images of sediment. Journal of Sedimentary Research 74 (1), 160–165.

Rubin, D.M., Chezar, H., Harney, J.N., Topping, D.J., Melis, T.S., Sherwood, C.R., 2006. Underwater microscope for measuring spatial and temporal changes in bed-sediment grain size. USGS Open –File Report 20061360, p. 15.

Rubin, D.M., Chezar, H., Harney, J.N., Topping, D.J., Melis, T.S., Sherwood, C.R., 2007. Underwater microscope for measuring spatial and temporal changes in bed-sediment grain size. Sedimentary Geology 202 (3), 402–408.

Ruggiero, P., Adams, P., Warrick, J., 2007. Mixed sediment beach processes: Kachemak Bay, Alaska. Coastal Sediments 2007. Vol. 1. ASCE, New Orleans, pp. 463–476.

Scott, D.W., 1992. Multivariate Density Estimation: Theory, Practice, and Visualization. Wiley, London.

Sheather, S., Jones, M., 1991. A reliable data-based bandwidth selection method for kernel density estimation. Journal of the Royal Statistical Society B 53, 683–690.

Silverman, B.W., 1986. Density Estimation. Chapman and Hall, London.

Sime, L.C., Ferguson, R.I., 2003. Information on grain sizes in gravel-bed rivers by automated image analysis. Journal of Sedimentary Research 73 (4), 630–636.

Stauble, D., 2007. Assessing beach fill compatibility through project performance evaluation. Coastal Sediments. Vol. 3. ASCE, New Orleans.

Weltje, G.J., Prins, M., 2003. Muddled or mixed? Inferring paleaoclimate from size distributions of deep sea clastics. Sedimentary Geology 162, 39–62.

Winkelmolen, A.M., 1982. Critical remarks on grain parameters, with special emphasis on shape. Sedimentology 29 (2), 255–265.